catalysts

MDPI

Article

Towards Photothermal Acid Catalysts Using Eco-Sustainable Sulfonated Carbon Nanoparticles—Part I: Synthesis, Characterization and Catalytic Activity towards Fischer Esterification

María Paula Militello, María Victoria Martínez, Luciano Tamborini, Diego F. Acevedo and Cesar A. Barbero *

Research Institute for Energy Technologies and Advanced Materials (IITEMA), National University of Río Cuarto (UNRC)-National Council of Scientific and Technical Research (CONICET), Río Cuarto 5800, Argentina; mmilitello@exa.unrc.edu.ar (M.P.M.); mmvictoriamartinez@gmail.com (M.V.M.); ltamborini@exa.unrc.edu.ar (L.T.); dacevedofernando@gmail.com (D.F.A.)

* Correspondence: cesarbarbero@gmail.com and cbarbero@exa.unrc.edu.ar; Tel.: +0054-3584028768

Abstract: The development of photothermal catalysts for biodiesel synthesis reaction (transesterification) requires the production of light-absorbing nanoparticles functionalized with catalytic (acid) groups. Using Stöber method, it is possible to produce resorcinol/formaldehyde resin (RF) nanoparticles, which can be carbonized (pyrolysis in an inert atmosphere) and sulfonated. In this work, vegetable tannins are used as a replacement for synthetic resorcinol in the Stöber synthesis of resin (TF) nanoparticles. The nanoparticles are characterized using DLS, FESEM, TEM and N_2 adsorption-desorption isotherms. Both resin and carbon nanoparticles are sulfonated by reaction with concentrated sulfuric acid. The attachment of sulfonic groups is verified by FTIR and EDX. The number of sulfonic groups is measured by acid/base titration and TGA. All sulfonated nanoparticles show catalytic activities towards Fischer esterification of ethanoic acid with ethanol, and high (up to 70%) conversion is obtained. The conversion is lower with TF-based nanoparticles, but the turnover numbers are similar in the RF- and TF-based materials. Sulfonated carbon and resin nanoparticles show higher catalytic activity compared to commercial acidic catalysts (e.g., Nafion®). Photothermal heating of carbon nanoparticles is observed. In Part II, sunflower oil transesterification, catalyzed by sulfonated nanoparticles, is observed. Photothermal catalysis of acetic acid esterification and sunflower oil transesterification is demonstrated.

Keywords: tannin/formaldehyde; nanoparticles; acid catalyst; sulfonation; biodiesel; esterification; photothermal

Citation: Militello, M.P.; Martínez, M.V.; Tamborini, L.; Acevedo, D.F.; Barbero, C.A. Towards Photothermal Acid Catalysts Using Eco-Sustainable Sulfonated Carbon Nanoparticles—Part I: Synthesis, Characterization and Catalytic Activity towards Fischer Esterification. *Catalysts* **2023**, *13*, 1341. https://doi.org/10.3390/catal13101341

Academic Editor: Diego Luna

Received: 1 September 2023
Revised: 21 September 2023
Accepted: 29 September 2023
Published: 4 October 2023

1. Introduction

The discovery of new catalysts allows the creation of new products or drastically improves the manufacture of important products, such as biofuels [1–5]. Many of the production processes of biodiesel currently designed and implemented in the industry are limited by high production costs due to the restrictions imposed by the chemical equilibrium, kinetics and the complexity of separation [6–9]. Heterogeneous catalysts, unlike homogeneous ones, are benign for the environment since they can be quickly separated from the product by filtration, regenerated and reused [10]. They have a high activity, selectivity and high tolerance to water [11]. They can be operated in continuous processes, which makes them promising for the reaction of transesterification of vegetable oils for the production of biodiesel, despite the high alcohol-to-oil molar ratio, large amounts of catalyst and high temperature and pressure required when using these catalysts on a large scale. Similar to homogeneous acid catalysts, heterogeneous catalysts can catalyze the reaction of esterification and transesterification. In a solid catalyst, the rate of reaction depends on the

access to active surface [12], but active sites are less accessible for the reactants, decreasing the catalyst's activity [13]. Several acidic heterogeneous catalysts have been studied such as cation exchange resins (e.g., Amberlyst-15 [14]), zeolites [15], sulfonated fluorinated polymers (e.g., Nafion® [16]) and mesoporous ordered silica (MCM-41 [17], SBA-15 [18]). Functionalized carbons can also be used as acidic catalysts for organic chemistry reactions (e.g., Fischer esterification [19,20]) [21–23]. Due to their large surface area, carbon nanoparticles could be used as heterogeneous catalysts. Moreover, given the transparency of the reaction media, carbon nanoparticles can be heated locally by light [24,25], producing photothermal catalysts.

The most widely used reagents in the synthesis of carbon precursor gels are resorcinol (R) and formaldehyde (F) [26] The polymerization of R and F occurs via a sol-gel reaction. Resorcinol reacts with formaldehyde to produce highly crosslinked polymers. The resorcinol molecule, or 1,3-dihydroxybenzene, which contains two hydroxyl groups (-OH) (Scheme 1), has three sites for electrophilic attack, which are 10 to 15 times more reactive than those corresponding to phenol, which has only one OH group. This contributes to the feasibility of forming RF polymers at relatively low temperatures. The sol-gel RF polymerization reaction (Scheme 1) begins with the formation of phenoxide anions by deprotonation by the base (Na_2CO_3, NH_4OH, etc.). This initial reaction results in the activation of the aromatic ring for the electrophilic aromatic substitution reaction on resorcinol by formaldehyde. Subsequent substitution reactions produce mainly hydroxymethyl groups on the aromatic ring, which subsequently condense to form methylene groups and methylene-ether bridges (Scheme 1). It can be seen that the second step involves the protonation of alcohol to form a carbocation. Therefore, weaker bases (e.g., Na_2CO_3) are more suitable for the whole reaction than strong bases (e.g., NaOH).

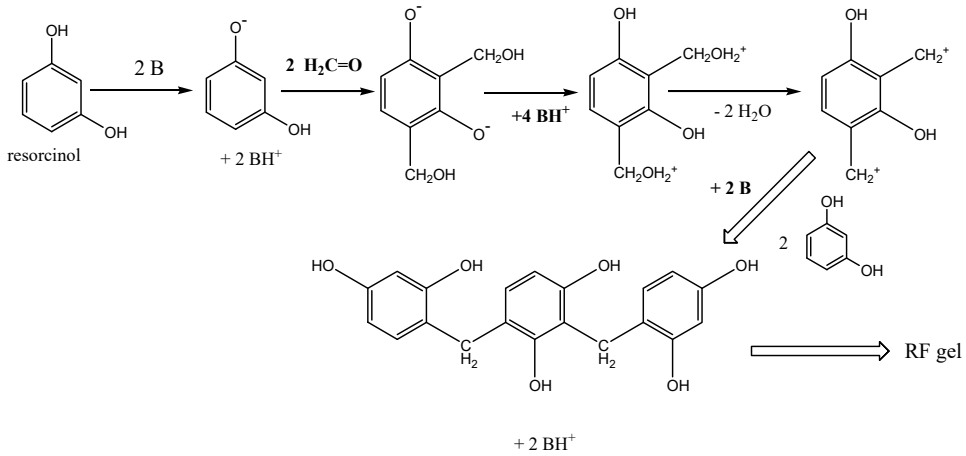

Scheme 1. Condensation reaction of resorcinol (R) with formaldehyde (F), catalyzed by a weak base.

There is a growing interest in the use of sustainable raw materials in the manufacture of catalysts [27,28], which allow a simple and economically viable synthesis to be industrialized. In the case of carbon catalysts derived from pyrolysis of polymeric resins, a suitable option to follow this sustainable trend is the replacement of synthetic precursors with natural precursors. Vegetable tannins (T) are complex substances of the phenolic type, with a relatively high molecular weight, which are widely distributed in the plant kingdom. They are present in the stems, leaves, seeds, fruits, bark and roots of many vegetables and constitute one of the natural products with the greatest industrial use, specifically in tanneries [29]. Tannins are not the same in all vegetables; they are complex polymers that differ in their composition and chemical properties according to the botanical genus where it is found. However, they have the advantage of being available in large quantities in nature, of being low-cost materials and friendly to the environment. Tannins present in their structure polyphenolic rings that are similar to resorcinol, for which they can substitute it in sol-gel reactions with formaldehyde. It has been shown that it is possible to

prepare tannin-based gels, and that in addition they are good precursors of carbonaceous materials [30]. Furthermore, the Argentine Republic is a large producer of tannins from trees (mainly from the autochthonous willow-leaf red quebracho, *Schinopsis balansae* [31]), which allows the incorporation of local resources into the manufacture of catalysts for the growing biodiesel industry.

The repeating units in tannins are generally linked together in positions 4 and 6 and/or 4 and 8 (Scheme 2) [32]. These units are repeated in the tannins, with a degree of polymerization approximating 4 to 5 [33]. This degree of polymerization suggests a polyphenolic chemical structure (Scheme 2) with a molecular weight of ca. 860 g/mol [34]. The existence of higher grade precursor molecules of condensation can be presented as an advantage at the time of the reaction, since it is they require fewer steps in sol-gel polymerization [35]. Moreover, each tannin unit contains a resorcinol-like subunit (**A**) and a pyrogallol-like subunit (**B**). The latter could also condense with formaldehyde to form a cross-linked resin, which makes it a potential precursor of carbon [36].

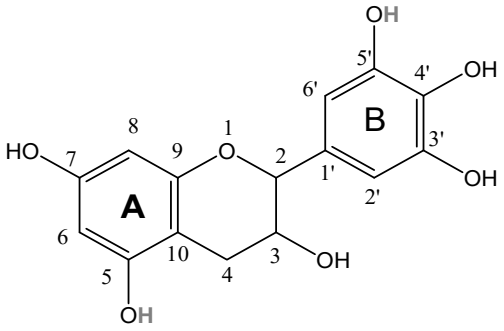

Scheme 2. Structure of the monomer unit of polymeric tannins.

The Stöber method is considered a particular approach to sol-gel processes, using which spheres of colloidal silica are produced by hydrolysis and condensation of alkoxides of silicon, such as TEOS, in aqueous solutions of alcohols and in the presence of a basic catalyst, usually ammonium hydroxide [37]. Using the Stöber method, it is possible to achieve precise control of particle size, narrow size distribution and smooth spherical morphology of the resulting silica, obtaining microporous silica [38] and mesoporous silica particles [39]. The method developed by Stöber can be extended for the preparation of monodisperse spherical particles of RF resin, with uniform and controllable particle size in the submicron scale [40,41].

In the present work, the synthesis and characterization of carbon nanospheres made by pyrolysis of resorcinol/formaldehyde and tannin/formaldehyde resin nanoparticles is described. The Stöber method is applied to produce the resin nanoparticles. Then, both resin and carbon nanoparticles are sulfonated. The attached sulfonic groups are detected by FTIR and EDX. The degree of modification is measured by titration, Boehm titration and TGA. The catalysts activity towards the esterification of ethanoic acid with ethanol is tested. The photothermal heating of carbon nanoparticles by light (NIR) irradiation is observed.

In Part II of this publication, the optimal parameters for Fischer esterification and sunflower oil transesterification (biodiesel synthesis) are obtained. Additionally, the photothermal catalysis of those reactions, by sulfonated carbon nanoparticles, is studied.

2. Results and Discussion

Resin nanoparticles (RF-x and TF-x) (see Materials and Methods) were synthesized by the Stöber method and characterized by different methods.

2.1. Characterization of Resin Nanoparticles by Dynamic Light Scattering (DLS)

The nanoparticles of resins synthesized by the Stöber route were analyzed by dynamic light scattering in order to characterize their size distribution (Figure 1).

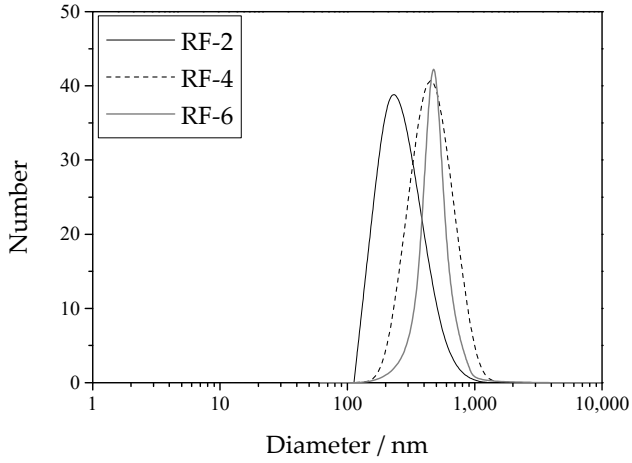

(A)

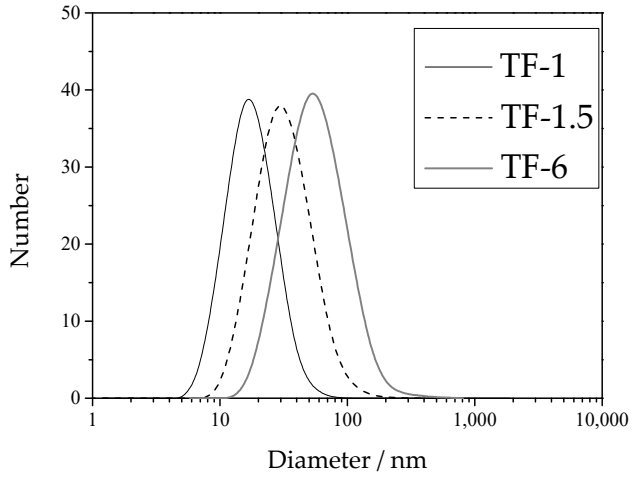

(B)

Figure 1. DLS measurement of the dispersions of RF (**A**) and TF (**B**) resin nanoparticles.

Table 1 shows the particle diameters, derived from the hydrodynamic radius, and polydispersity indices (PIs) of the polymeric resins derived from both systems, RF and TF. The dynamic light scattering measurements were performed only on the carbon precursor resins because, in the laser emission zone of the DLS equipment, the carbon absorbs radiation, and therefore the measurement on the carbon is not reliable in a pyrolyzed material.

Table 1. Particle diameters (dP/nm) and polydispersity indices (PIs) determined by DLS for RF-x and TF-x polymeric resins.

Material	dP	PI
RF-2	270	0.6
RF-4	490	0.3
RF-6	520	0.1
TF-1	20	0.5
TF-1.5	35	0.5
TF-6	65	0.5

The RF-6 resins have the lowest polydispersity index, which increases at smaller sizes when the R:A ratio decreases. In the case of TF-x resins, whose sizes are less than 100 nm, it should be noted that they have a PI of 0.5 in all cases, without presenting a clear correlation between the PI and dP values. Figure 1A shows the particle size distribution for the materials synthesized from resorcinol and formaldehyde. In it, the difference in the width of the dP distribution bell that exists between the RF-x materials is clear, with the RF-6 polymer resin presenting the narrowest distribution, in accordance with the PI value obtained. Figure 1B, shows the size distribution for resins of the tannin-formaldehyde precursor systems, clearly indicating the high polydispersity index that this type of material exhibits. However, all of the TF-x resins synthesized have a particle size of less than 100 nm, which makes them potential support materials for nanocatalysts. The resin nanoparticles are pyrolyzed in an inert atmosphere to produce carbon nanoparticles (CRF and CTF). Due to the high optical absorption of the carbon nanoparticles at the wavelength of the laser beam (432 nm), DLS measurements of the carbon nanoparticles are not possible. Therefore, SEM and TEM were used to measure the size of carbon nanoparticles.

2.2. Characterization of Carbon Nanoparticles by FE-SEM

Carbon materials derived from the RF and TF precursor systems were studied by FE-SEM. Figure 2 shows the micrographs obtained by this technique. As can be seen in (a) and (b) micrographs (Figure 2), corresponding to CRF-6/600, the material presents spherical morphology, with a narrow particle size range around 550 nm. These properties determined by SEM agree closely with that provided by dynamic light scattering measurements, performed on the resin nanoparticles from which these carbon materials are derived. It is somewhat surprising that very little shrinkage of the material (resin) to carbon is observed. It is known that monolithic pieces of RF resins [42], decrease the volume up to 40% upon carbonization. However, porous resin could increase density in the solid mass with increasing porosity and not volumetric shrinkage.

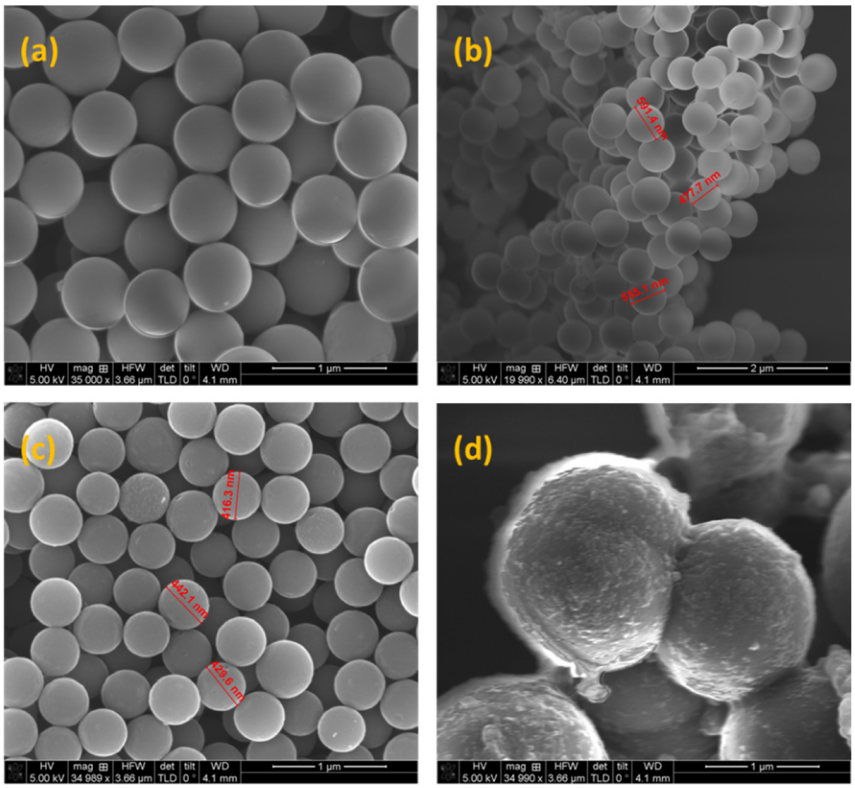

Figure 2. FE-SEM micrographs of (**a**,**b**) CRF-6/600, (**c**) CRF-4/600 and (**d**) CTF-1/600.

In the same way, these properties can be observed in micrograph (c) for the CRF-4 material, which differs from the previous one in the concentration of organic precursors, R and F, in the reaction medium. Therefore, the particle size of this material is smaller, since it comes from a lower concentration reaction mixture. The average particle size, in the latter case, ranges from 450 nm. Of greater interest is micrograph (d), corresponding to CTF-1. In this image it can be seen that the particles are larger, greater than 1 µm, and that they also appear to be agglomerated. Although they present a spherical morphology, the surface presents a roughness that is not visualized in materials from the RF systems. On the other hand, the size is considerably larger than that obtained by DLS, whose previously reported value was approximately 60 nm. The difference is that to carry out the dynamic light scattering measurements, the reaction product is centrifuged, and a supernatant is analyzed, which in this case turns out not to be representative of the wide size dispersion obtained.

2.3. Transmission Electron Microscopy (TEM) of Carbon Nanoparticles

Transmission electron microscopy measurements were performed on the synthesized carbon materials in order to obtain additional information about their morphology. Figure 3 shows a micrograph of the CRF-6/600 material obtained using the TEM equipment at 200 keV.

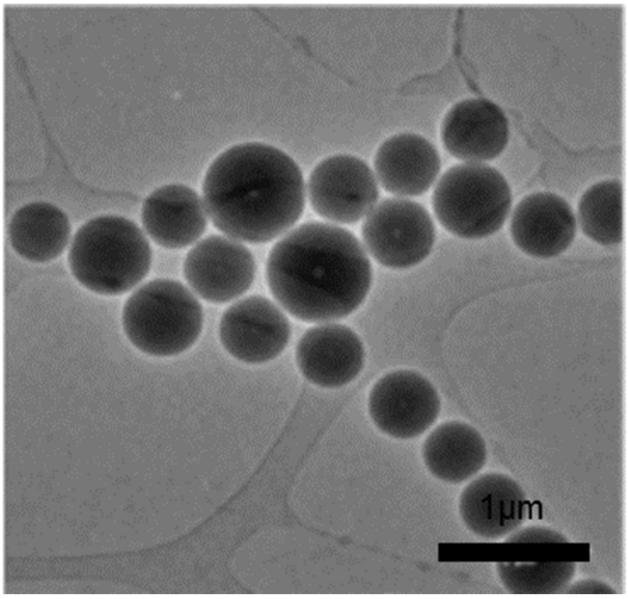

Figure 3. TEM micrograph of CRF-6/600 at 200 keV.

It can be clearly observed that the morphology of the nanoparticles is spherical. Therefore, the DLS measures true size since the calculation assumes a spherical morphology. In addition, it can be seen that there is a certain distribution of particle sizes (between 400 and 800 nm), with the mean size at 480 nm. Taking into account that the resin from which this carbon comes presents a dP around 550 nm, determined by DLS, the maximum reduction in this dimension during pyrolysis can be considered approximately 14%.

The textural properties of the surface of the particles are related to the tendency of the material to continue polymerizing until gelation is reached. It has been observed that the RF-x particles can be stored in colloidal suspension, even without being separated from the reaction medium, for weeks, while the TF-x resins, after a few days, begin to agglomerate until they gel. The CRF-6 nanospheres have practically zero porosity, as can be seen in Figure 4.

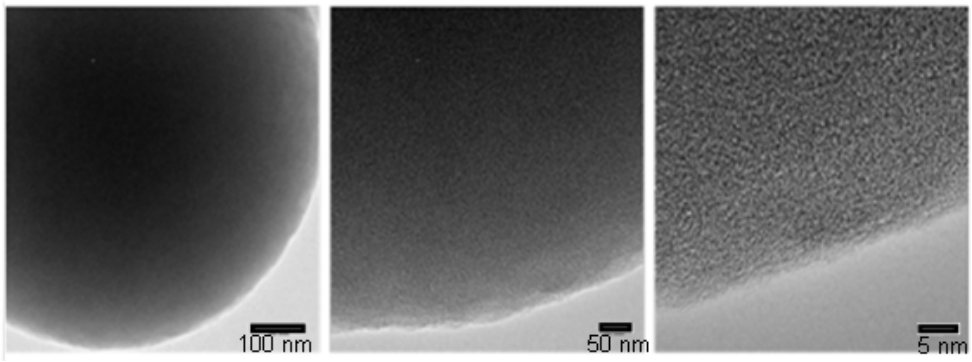

Figure 4. TEM micrographs of a CRF-6/600 particle at 200 keV.

2.4. Nitrogen Adsorption–Desorption Isotherms

Measurements of nitrogen adsorption-desorption isotherms were carried out in order to characterize the textural properties of carbons and resins, both from the RF and TF precursor systems. In this way it was also possible to know the effects of the pyrolysis on the materials structure.

From the observation of the nitrogen adsorption-desorption isotherms in Figure 5, it is possible to ensure that the isotherms are of type II, and therefore we have nonporous materials. In the analysis, there is physical multilayer adsorption and a total absence of hysteresis in the adsorption-desorption cycle, so the process is completely reversible. This occurs for the materials analyzed, resin and carbon. It can be concluded that the pyrolysis process does not modify the porous structure of the material. The results obtained from the nitrogen adsorption-desorption analysis of RF-6, CRF-6/600, TF-1 and CTF-1/600, applying BET theory and density functional theory (DFT) for the calculations, are summarized in Table 2 As can be seen in Table 2, the samples analyzed exhibit a very low surface area, which agrees with the observation, from their isotherms, that they are nonporous materials with low microporosity. Comparing the resin and carbon nanoparticles, it can be seen that pyrolysis causes an increase in surface area associated with a decrease in particle size and a decrease in the density of the material. Although the software used shows pore diameter values, they are below the reliability limit of the equipment used and therefore not representative of the textural properties of the analyzed materials.

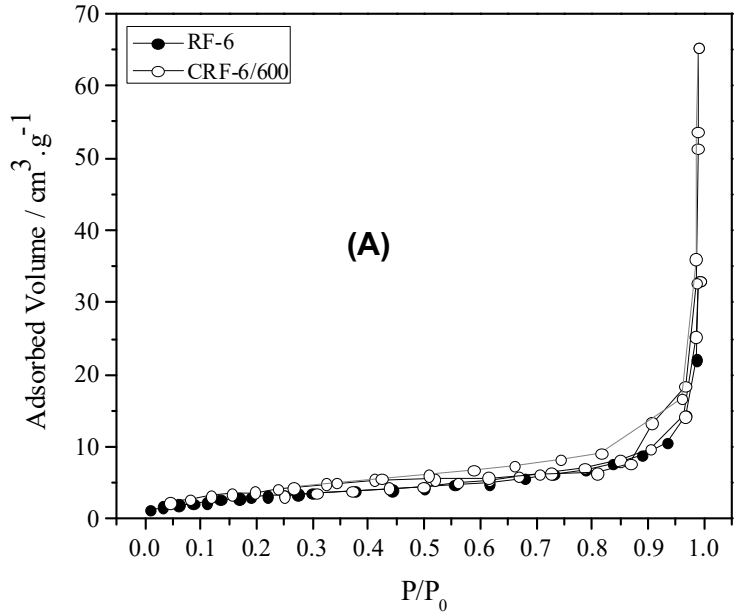

Figure 5. *Cont.*

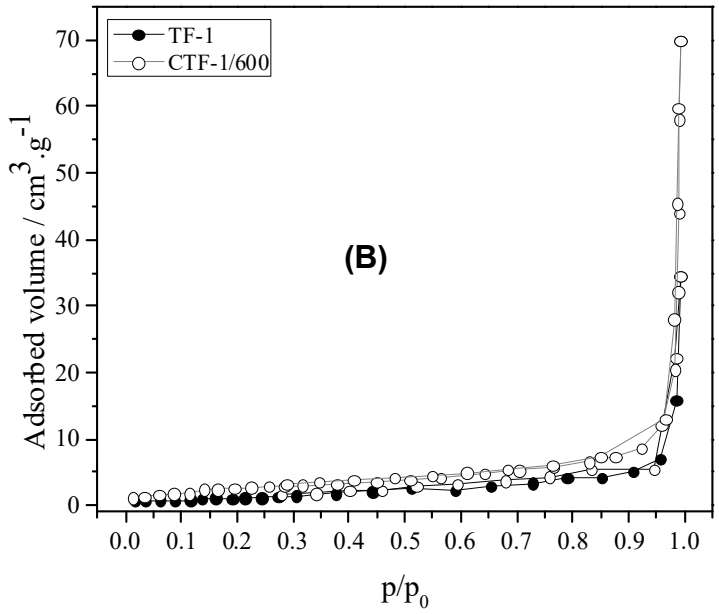

Figure 5. (**A**) Nitrogen adsorption-desorption isotherms at 77 K of RF-6 and CRF-6/600. (**B**) Nitrogen adsorption-desorption isotherms at 77 K of TF-1 and CTF-1/600.

Table 2. Results obtained from the analysis of nitrogen adsorption-desorption isotherms at 77 K for RF, CRF, TF and CTF materials.

Material	S_{BET} [a] (m^2/g)	V_{mic} [b] (cm^3/g)	V_{meso} [b] (cm^3/g)	V_t [b] (cm^3/g)	Dp [c] (nm)
RF-6	11.70	0.004	0.047	0.051	1.5
CRF-6/600	15.13	0.007	0.094	0.101	2.7
TF-1	3.38	0.002	0.051	0.053	2.8
CTF-1/600	9.43	0.003	0.105	0.108	2.8

[a] Determined using BET mode, [b] determined using ASiQwin software, 2.1 [c] determined using DFT.

In Table 2, it can be seen that the samples analyzed, similar to those from the RF systems, exhibit a very small surface area in agreement with what was observed from their adsorption-desorption isotherms, since they are nonporous materials. It is concluded from this analysis that the particles synthesized by the Stöber method constitute nonporous or very low porosity materials, whose accessible surface area is basically given by the particle external area.

2.5. Synthesis of Sulfonated Nanoparticles

The polymeric resin and carbon nanoparticles derived from their pyrolysis, were functionalized by reaction with concentrated sulfuric acid (see experimental part). After performing the sulfonation of the previously described materials, the anchoring of sulfonic groups to the carbon surface was studied by FTIR spectroscopy and compositional analysis (EDX).

2.6. FTIR Spectroscopy

Using FTIR spectroscopy, the covalent binding of the sulfonic groups to the surface of the functionalized materials was verified. The materials CRF-6/600 and CRF-6/600/H_2SO_4/80 were chosen as representative of the set of carbons synthesized to exemplify the results obtained. The spectra obtained for the mentioned materials are shown in Figure 5. Although the FTIR spectra were taken between 4000 and 500 cm^{-1}, the figure shows only the region corresponding to the fingerprint of the materials and the main absorption bands present.

In Figure 6, it can be seen that the infrared spectrum of the sulfonated carbon presents bands that are not found in the spectrum of the non-sulfonated carbon. At 1068 cm^{-1}, the CRF-6/600/H_2SO_4/80 material shows a band attributed to the sulfonic group. In addition, bands attributable to the S=O stretch are clearly seen at 1015 and 1176 cm^{-1}. Moreover, a band is observed at 580 cm^{-1} that is assigned to the C-S stretch [43]. The assignment of bands observed in the FTIR spectra are summarized in Table 3. The results suggest the anchoring of the sulfonic groups to the materials.

Table 3. Absorption bands present in the infrared spectrum of sulfonated carbon CRF-6/600/H_2SO_4/80.

Wavenumber (cm^{-1})	Intensity	Vibration	Functional Group	
1322	Medium	Stretch	R–SO_2–R	Asymmetric
1287	Medium	Stretch	O=S=O	Asymmetric
1176	Strong	Stretch	O=S=O	Symmetric
1070	Medium	Stretch	–SO_3H	Sulfonic
1015	Medium	Stretch	S=O	Sulfonic
852	Medium	Stretch	–C–S–	Aromatic
675	Weak	Bending	–S–O–	Sulfonic
615	Medium	Bending	–S–OH	Sulfonic
580	Medium	Stretch	C–S	Sulfonic

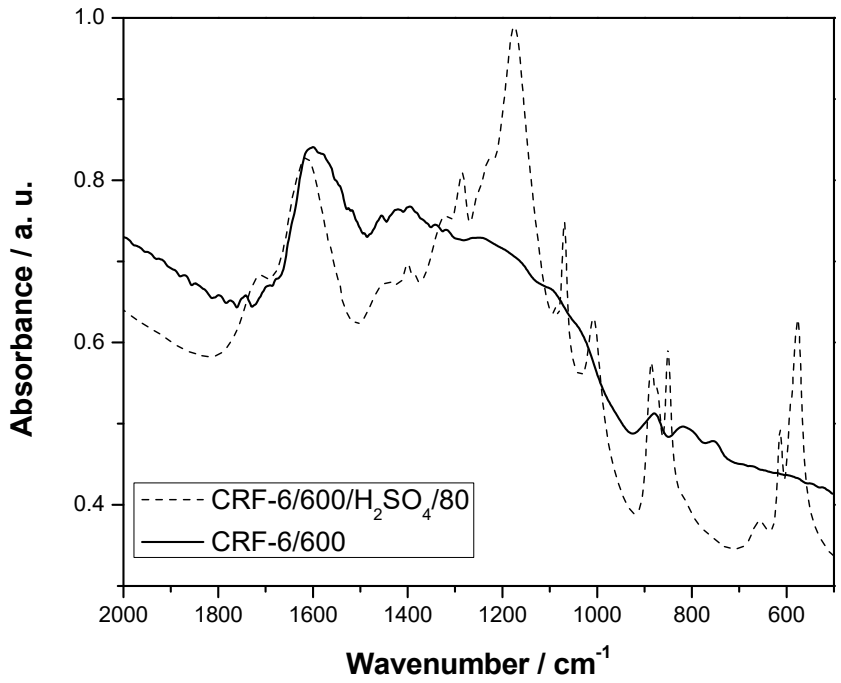

Figure 6. FTIR spectra of CRF-6/600 and CRF-6/600/H_2SO_4/80 in the region 2000 at 500 cm^{-1}.

2.7. Compositional Characterization by SEM-EDX

SEM-EDX measurements were performed for CRF-6/600 and CRF-6/600/H_2SO_4/80 samples and for CTF-1/600 and CTF-1/600/H_2SO_4/80 samples. With this technique, the detection of elements (e.g., S) in the added groups could be carried out (Figure S5, Supplementary Materials).

The data shown in Table 4 clearly agree with the anchoring of sulfonic groups on the carbon materials after sulfonation. The elemental maps from EDX (Figures S6–S9 in the Supplementary Materials) show uniform distribution of S, suggesting that the sulfonation is uniform.

Table 4. Elemental composition obtained by EDX for CRF-6/600 and CRF-6/600/H_2SO_4/80.

Element	% Weight	% Atoms	% Weight	% Atoms
	CRF-6/600		CRF-6/600/H_2SO_4/80	
C	84.24	87.64	76.11	81.27
O	15.76	12.36	22.85	18.32
S	0	0	1.04	0.42
	CTF-1/600		CTF-1/600/H_2SO_4/80	
C	93.99	95.42	56.82	65.51
O	6.01	4.58	36.56	31.64
S	0	0	6.62	2.86

2.8. Determination of the Functionalization Degree (nGS) by Potentiometric Titration

Once the effective functionalization of the materials was verified, the content of sulfonic groups was determined by acid-base potentiometric titration. The application of this technique was carried out both on the resins and on the carbons derived from them, after either direct sulfonation, with sulfuric acid as a sulfonating agent, or mediated by diazonium salts. Once the content of sulfonic groups in each material was determined, the influence that different variables have on the nGS value was analyzed. These variables were the sulfonation method used and the Tp applied in the carbonization cycle of the resins.

2.9. Influence of the Precursor System on nGS

The nGS measurements were made for sulfonated RF and TF carbons and resins by the methods described in the experimental part. In Figure S4 (Supplementary Materials), the titration curves obtained for sulfonated resins from the RF and TF systems are presented, functionalized by direct sulfonation techniques with H_2SO_4 (RF-6/H_2SO_4/50 and TF-1/H_2SO_4/50). The sulfonation level also varies from one precursor system to another: it is higher in the case of resins from the RF reaction systems. Although the results expressed in the graph represent only the values of TF-1 and RF-6, this is so because these catalysts were the ones with the highest number of active functional groups on their surface compared to other TF-x and RF-x catalysts, respectively. However, the trend was observed for all resins functionalized by both methods, as can be seen in Table 5, where the nGS values for all sulfonated resins are expressed.

Table 5. Content of sulfonic groups by acid-base potentiometric titration of nanoparticles of sulfonated resins (RF and TF) and carbons (CRF an CTF) [a].

Material	nGS (mmol/g)
RF-6/H_2SO_4/50	11.83
RF-4/H_2SO_4/50	11.77
TF-1/H_2SO_4/50	8.33
TF-1.5/H_2SO_4/50	7.92
TF-6/H_2SO_4/50	7.9
CRF-6/600/H_2SO_4/80	8.99
CRF-4/600/H_2SO_4/80	7.03
CTF-1/600/H_2SO_4/80	7.62
CTF-1.5/600/H_2SO_4/80	7.11
CTF-6/600/H_2SO_4/80	6.95

[a] Titrant solution = 0.05 M NaOH.

The effect of the precursor, observed for the pyrolyzed materials prior to sulfonation, is the same as that determined for the resins: the sulfonation level is higher when the material comes from the RF reaction systems. This is possibly related to the structure of the material, differences in porosity and surface texture, exposed groups in the starting materials, etc. On the other hand, tannins have abundant -COR groups in their structure, which constitute deactivating groups in electrophilic aromatic substitution, a mechanism followed by sulfonation with sulfuric acid. This can bring about, then, a decrease in the degree of sulfonation that these TF-x and CTF-x materials present in relation to RF-x and CRF-x, respectively. The content of sulfonic groups is considerably higher for the resin samples in reference to the carbons derived from them. This is reasonable considering that the effectiveness of electrophilic sulfonation should be higher in phenolic (resin) rings than in benzenoid graphene (carbon) rings. The results also indicate that the RF-6/H_2SO_4/50 and CRF-6/600/H_2SO_4/80 catalysts have the highest content of sulfonic groups, for which the RF precursors are potentially better for obtaining functionalized carbon materials with sulfonic groups. In all cases, the acid group content found for the materials synthesized is higher than that of materials commonly used as esterification catalysts, including commercial catalysts such as exchange resins: Amberlite IR-120 (4.6 mmol/g), Nafion 117 (0.9 mmol/g) or sulfonated carbon (Starbons-300-H_2SO_4-15, 1.1 mmol/g) [44]. The nGS values are higher in the case of the RF-6/H_2SO_4/50 and CRF-6/600/H_2SO_4/80 catalysts. The fact of exhibiting a higher content of sulfonic groups makes materials with an R:A ratio of 6 the best candidates for acid catalysts.

2.10. Influence of Resin Pyrolysis Temperature on nGS

The content of sulfonic groups (nGS) of carbon materials obtained by two different pyrolysis cycles was evaluated by potentiometric titration, in order to determine if this variable has an effect on the final degree of functionalization achieved. The motivation for this analysis lies in the fact that the heating cycle and final temperature in pyrolysis have direct effects on the graphitic structure of the obtained carbon and the number of oxygen groups remaining on its surface. The structural differences can cause, then, differences in the degrees of anchorage of sulfonic groups and their stabilization. Table 6 shows the contents of sulfonic groups obtained by acid-base potentiometric titration for sulfonated carbon materials, obtained by both pyrolysis cycles and sulfonated by reflux with H_2SO_4. Also included in the said table are the nGS values corresponding to the precursor resins, functionalized by the same route. Based on the results tabulated in the table, it can be said that the calcination temperature does not have a significant influence on the subsequent yield of the sulfonation.

The values obtained for nGS in carbons derived from pyrolysis at 900 °C are very close to those obtained for carbons pyrolyzed at 600 °C. In most cases, they are somewhat lower. The largest difference is only 13% and occurs between the CRF-6/600/H_2SO_4/80 and CRF-6/900/H_2SO_4/80 materials. The contrast observed may be due to the uneven structure of the carbon that is reached at different pyrolysis temperatures of the material. When the heat treatment is carried out at a higher temperature, the carbonization of the material is more complete, which is why the material has fewer phenolic rings, characteristic of the resin, and more graphene benzene rings. The effectiveness of electrophilic sulfonation is greater in phenolic rings, so materials with a lower degree of carbonization present a higher degree of sulfonation.

2.11. Determination of nGS by Thermogravimetric Analysis (TGA)

The results obtained by potentiometric titration of sulfonic groups for the materials CRF-6/600/H_2SO_4/80 and CRF-6/900/H_2SO_4/80 were compared with thermogravimetric (TGA) measurements. A heating ramp was used as the one shown in Figures S2 and S3 (Supplementary Materials). The initial temperature for the experiments was 25 °C and it rose at a rate of 10 °C/min, until 500 °C is reached, temperature at which the sample to be analyzed was maintained for 15 min. The curves derived from the thermogravimetric

analysis for the different materials are shown in Figure 7. In both curves in the graph show that there are two steps of mass loss: the first step starts near 100 °C, and the later one between 200 and 350 °C. The first decay is attributable to a loss of water present in the sample, due to the hydrophilicity of the functional groups on the carbon surface. The second decrease in the mass percentage is due to the degradation of the sulfonic groups that each of the analyzed materials possesses.

Table 6. Content of sulfonic groups obtained by potentiometric titration for sulfonated resins and sulfonated carbons.

Material	Temperature of Pyrolysis (°C)	nGS (mmol/g)
RF-6/H_2SO_4/50	None	11.83
CRF-6/600/H_2SO_4/80	600	8.99
CRF-6/900/H_2SO_4/80	900	7.83
RF-4/H_2SO_4/50	None	11.77
CRF-4/600/H_2SO_4/80	600	7.03
CRF-4/900/H_2SO_4/80	900	7.11
TF-1/H_2SO_4/50	None	8.33
CTF-1/600/H_2SO_4/80	600	7.62
TF-1/900/H_2SO_4/80	900	7.2
TF-1.5/H_2SO_4/50	None	7.92
CTF-1.5/600/H_2SO_4/80	600	7.11
CTF-1.5/900/H_2SO_4/80	900	7.24
TF-6/H_2SO_4/50	None	7.9
CTF-6/600/H_2SO_4/80	600	6.95
CTF-6/900/H_2SO_4/80	900	6.72

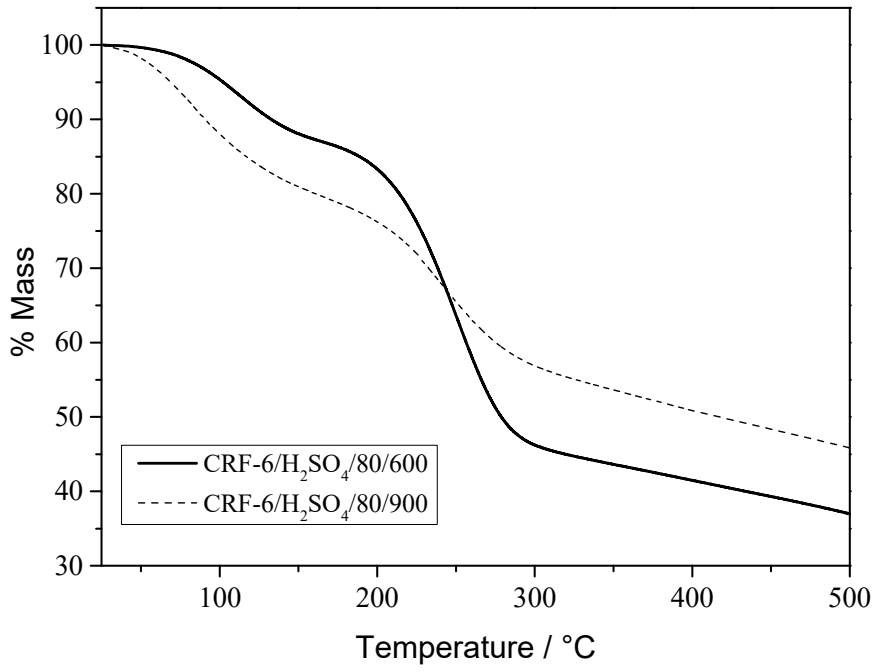

Figure 7. Curves obtained by TGA in a nitrogen atmosphere to determine the content of sulfonic groups in CRF-6/H_2SO_4/80/600 and CRF-6/H_2SO_4/80/900.

In the case of CRF-6/600/H_2SO_4/80, the mass loss due to degradation of the sulfonic groups reaches a value of approximately 50%, while the moisture loss is 12%. For the CRF-6/900/H_2SO_4/80 material, the mass loss due to degradation of the functional groups reaches a value of 36%, while the moisture loss is 18%. With these data, it is possible to calculate the content of sulfonic groups per gram of dry material contained in the samples. Table 7 lists the results obtained for both samples analyzed. As can be observed from the table, the content of sulfonic groups calculated from the data provided by this technique differs from the values obtained by potentiometric titration (ca. 7% for CRF-6/H_2SO_4/80/600 and ca. 18% for CRF-6/H_2SO_4/80/900). In that way, the lower degree of sulfonation of the material calcined at a higher temperature is also verified. The discrepancy between the nGS values obtained by both methods may be due to the fact that in the thermogravimetric analysis the heating ramp reached an insufficient temperature for the degradation of all the sulfonic group content. Some data on similar materials [45,46], where pyrolysis temperatures exceed 700 °C, show species which may be lost at higher temperatures, causing errors in the measurement. In our measurements, only 500 °C is reached due to experimental constraints (stability of the crucible). The heat treated samples show traces of sulfur (EDX), suggesting that not all the sulfonic groups have been removed at 500 °C.

Table 7. Content of sulfonic groups in CRF-6/600/H_2SO_4/80 and CRF-6/900/H_2SO_4/80 obtained by thermogravimetric analysis.

Material	CRF-6/600/ CRF-6/600/H_2SO_4/80	CRF-6/900/H_2SO_4/80
Initial Mass (mg)	35	35
%Wwater loss	12	18
%Wloss –SO3H	51	36
Mass of water lost (mg)	4.2	6.3
Mass of –SO_3H lost (mg)	17.85	12.6
Moles –SO_3H lost (mmol)	0.22	0.156
Dry material mass (mg)	30.8	28.7
nGS (mmol/g)	7.14	5.45

2.12. Boehm Titration: Content of Total, Phenolic, Lactonic and Carboxylic Acid Groups

The Boehm method comprises a series of back titrations, in which bases of different basic strength are used, which makes it possible to determine the individual content of different acid groups present on the surface of carbon materials. The method was applied on samples RF-6/H_2SO_4/50, CRF-6/600/H_2SO_4/80, TF1/H_2SO_4/50 and CTF-1/600/H_2SO_4/80, which exhibit a higher content of sulfonic groups among the synthesized samples for each of the precursor systems (Table 8).

Table 8. Content of total acid (nGT), sulfonic (nGS), carboxylic (nGC), lactonic (nGL) and phenolic (nGP) groups of sulfonated resins and carbons, determined by the Boehm method (mmol/g).

Material	nGT	nGS	nGC	nGL	nGP
RF-6/H_2SO_4/50	12.24	11.83	0.09	0.15	0.17
CRF-6/600/H_2SO_4/80	11.97	8.99	1.17	0.96	0.85
TF-1/H_2SO_4/50	8.77	8.33	0.12	0.13	0.19
CTF-1/600/H_2SO_4/80	8.29	7.62	0.25	0.2	0.22
TF-1.5/H_2SO_4/50	8.49	7.92	0.1	0.12	0.35
CTF-1.5/600/H_2SO_4/80	7.78	7.11	0.21	0.18	0.28
TF-6/600/H_2SO_4/50	8.32	7.9	0.09	0.12	0.21
CTF-6/H_2SO_4/80	7.51	6.95	0.16	0.16	0.24

By means of these acid-base titrations based on the Boehm method, the acid sites present in the catalysts of interest were completely characterized, those with the highest

content of sulfonic groups in each of the precursor systems. Although the acid group content of the tannin-formaldehyde carbon has fewer acid sites than that from resorcinol-formaldehyde, this number is significant and comparable to that of commercial catalysts. Values of nGT and nGS for CRF-x/600/H_2SO_4/80 and CTF-x/600/H_2SO_4/80 are tabulated in Table 9, together with the values obtained for mesoporous carbon materials published by Aldana-Pérez et al. [44] in order to compare the content of the acid groups.

It should be noted that, unlike the commercial carbons used in the comparison, the CRF-x and CTF-x carbons do not present developed mesoporosity, which implies that the number of sulfonic groups per unit of the exposed area of the material will be hundreds of times higher, according to morphological and textural studies carried out using TEM and nitrogen adsorption-desorption isotherms. Moreover, while the Starbon carbon material shows a low percentage of –SO_3H groups (%S/T < 25%) in the total number of acidic groups (-OH, –COOH, –SO_3H), the sulfonated materials' nanoparticles synthesized here are mostly sulfonated (% S/T > 60%), since strongly acidic sulfonic groups are better catalysts for Fischer esterification than weakly acidic phenolic or carboxylic groups, and optimum material should have a large number of sulfonic groups.

Table 9. Number of total acid (nGT) and sulfonic (nGS) groups of CRF-x/600/H_2SO_4/80 and CTF-x/600/H_2SO^4/80 carbon and Starbon 300 commercial carbon (sulfonated with sulfuric acid and sulfuric acid mixtures and chlorosulfonic acid) in mmol/g [44] with % of sulfonic group in the total acid groups (%S/T).

Material	nGT	nGS	%S/T
CRF-6/600/H_2SO_4/80	11.9	9	76
CRF-4/600/H_2SO_4/80	11.7	7	61
CTF-1/600/H_2SO_4/80	8.3	7.6	92
CTF-1.5/600/H_2SO_4/80	8.4	7.8	93
CTF-6/600/H_2SO_4/80	7.8	7.5	96
Starbons-300-H_2SO_4-15	8	1.1	14
Starbons-300-2-$ClSO_3H$-H_2SO_4-5	8.2	1.8	22
Starbons-300-3-$ClSO_3H$-H_2SO_4-5	10	2.3	23

2.13. Nitrogen Adsorption–Desorption Isotherms of Sulfonated Nanoparticles

Figure 8 shows the nitrogen adsorption-desorption isotherms of (A) RF-6 and RF-6/H_2SO_4/50 and (B) CRF-6/600 and CRF-6/600/H_2SO_4/80. From the analysis of these graphs, it can be affirmed that the isotherms are of type II and present, in all the cases, a very small hysteresis loop in the adsorption-desorption, so the process is mostly reversible. This occurred for the four materials analyzed; therefore, it can be concluded that the pyrolysis and sulfonation processes do not confer appreciable changes to the materials in their textural properties.

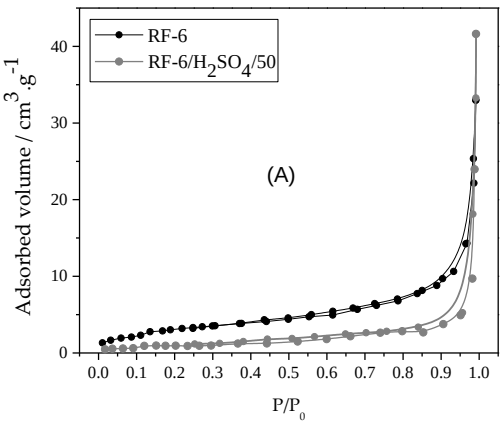

Figure 8. *Cont.*

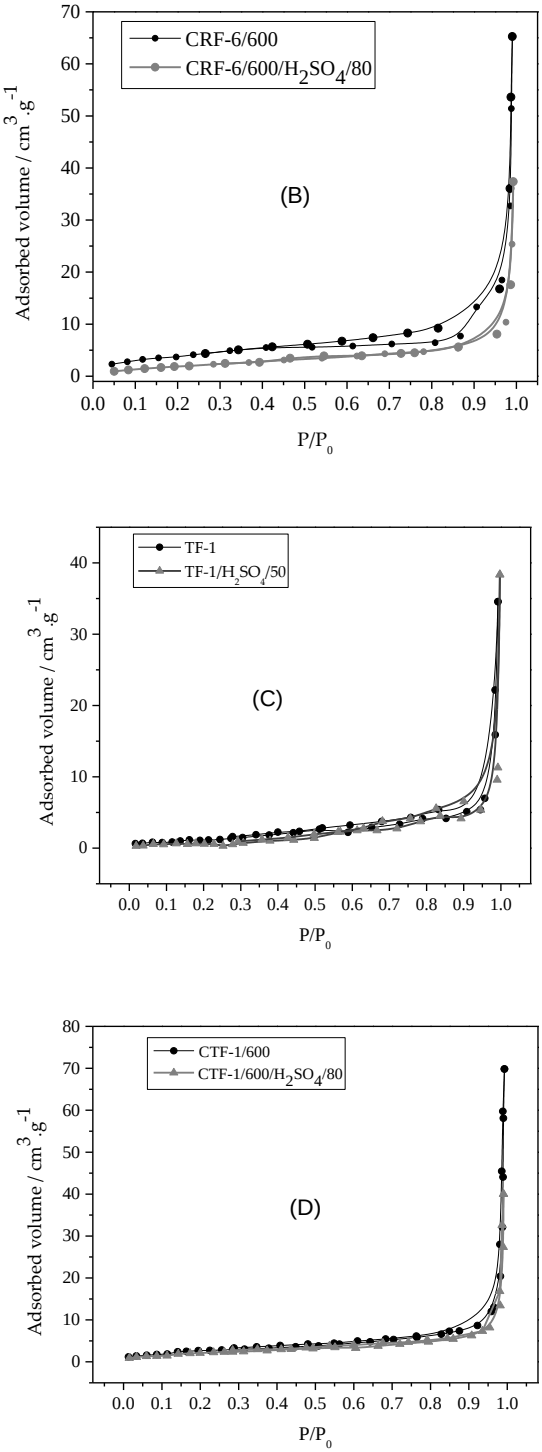

Figure 8. Nitrogen adsorption-desorption isotherms at 77 K of (**A**) RF-6 and RF-6/H_2SO_4/50 and (**B**) CRF-6/600 and CRF-6/600/H_2SO_4/80. Nitrogen adsorption-desorption isotherms at 77 K of (**C**) TF-1 and TF-1/H_2SO_4/50 and (**D**) CTF-1/600 and CTF-1/600/H_2SO_4/80.

The results obtained from the nitrogen adsorption-desorption analysis for the RF-6, RF-6/H_2SO_4/50, CRF-6/600 and CRF-6/600/H_2SO_4/80 materials, applying the BET theory and DFT for the calculations, are summarized in Table 10.

Table 10. Results obtained from the analysis of nitrogen adsorption-desorption isotherms at 77 K for RF-6, RF-6/H_2SO_4/50, CRF-6/600 and CRF-6/600/H_2SO_4/80.

Material	S_{BET} [a] (m^2/g)	V_{mic} [b] (cm^3/g)	V_{meso} [b] (cm^3/g)	V_t [b] (cm^3/g)	Dp [c] (nm)
RF-6	11.7	0.004	0.047	0.051	1.5
RF-6/H_2SO_4/50	3.11	0.001	0.063	0.064	1.5
CRF-6/600	15.13	0.007	0.094	0.101	2.7
CRF-6/600/H_2SO_4/80	8.27	0.004	0.054	0.058	2.6

[a] Determined using BET theory, [b] determined using ASiQwin software, [c] determined using DFT.

As can be seen in Table 10 all the samples analyzed exhibit a very low surface area, which agrees with the observation, from their isotherms, that they are materials with very low or no porosity. Comparing the materials RF-6 and CRF-6/600/H2SO4/80, the results indicate that sulfonation induces a decrease in the surface area (S_{BET}), both of the resin and of the carbon, due to an increase in the weight of the material, but it does not apparently affect the average pore diameter calculated by DFT.

2.14. Nitrogen Adsorption–Desorption Isotherms of TF Materials

Figure 6 shows the nitrogen adsorption-desorption isotherms of (C) TF-1 and TF-1/H2SO4/50 and (D) CTF-1/600 and CTF-1/600/H_2SO_4/80. As in the case of the RF materials, there is no hysteresis loop in adsorption-desorption in any of the analysis cases. Therefore, it can be concluded that the sulfonation process does not modify the porous structure of the material. The results obtained from the nitrogen adsorption-desorption analysis for these materials are summarized in Table 11. It can be seen that the samples analyzed, similar to those of the RF systems, exhibit a very small surface area in agreement with what was observed from their adsorption-desorption isotherms, since they are materials without developed porosity. In this type of material, a decrease in ABET is observed, caused by sulfonation, both of the resin and of the carbon, due to an increase in the weight of the material. The average pore diameter calculated by DFT is not noticeably affected in either of the two sulfonation processes.

Table 11. Results obtained from the analysis of nitrogen adsorption-desorption isotherms at 77 K for TF-1, TF-1/H_2SO_4/50, CTF-1/600 and CTF-1/600/H_2SO_4/80.

Material	S_{BET} [a] (m^2/g)	V_{mic} [b] (cm^3/g)	V_{meso} [b] (cm^3/g)	V_t [b] (cm^3/g)	Dp [c] (nm)
TF-1	3.38	0.002	0.051	0.053	2.8
TF-1/H_2SO_4/50	2.12	0.001	0.058	0.059	5.2
CTF-1/600	9.43	0.003	0.105	0.108	2.8
CTF-1/600/H_2SO_4/80	7.77	0.003	0.059	0.062	2.8

[a] Determined using BET theory, [b] determined using ASiQwin software, [c] determined using DFT.

2.15. Catalytic Activity of Nanoparticles

The catalytic activity of the synthesized materials was studied by the Fischer esterification reaction kinetics; one of the reagent systems selected for this was made up of acetic acid and methanol. In the first place, the importance that sulfonation has on the catalytic activity of carbon was analyzed. For this, the performance of the synthesized materials was evaluated before and after functionalization. Figure 7 shows the results obtained for the CRF-6/600 and CRF-6/600/H_2SO_4/80 samples.

The results shown in the graph of Figure 9 suggest that both the precursor phenol (resorcinol or tannin) and carbonization affect the catalytic capacity of the materials. Resorcinol-based catalysts induce large conversions (ca. 70%) and similar behavior between the resin and carbon particles (Figure 9A). On the other hand, tannin-based catalysts show smaller maximum conversions (up to 60%) and larger differences between the carbon (higher conversions) and resin nanoparticles (lower conversions). However, the num-

ber of catalytic groups (-SO_3H) depend on the precursor and carbonization. Plotting the turnover number (TON), which is the mmol of acetic acid converted per each sulfonic group (Figure 10), provides a clearer picture.

If the conversion achieved by the number of sulfonic groups is normalized, the turnover number (TON) graph is obtained as a function of time, as shown in Figure 10. This type of graph is more representative of the effectiveness that the sulfonic groups of each material have to catalyze the Fischer esterification reaction. In Figure 8, the greater effectiveness of the acid groups of the carbonized material to catalyze the esterification reaction remains relevant. It is also observed that, although the content of sulfonic groups in CTF-1/600/H_2SO_4/80 is lower than that in CRF-6/600/H_2SO_4/80 (8.99 and 7.62 mmol/g, respectively), both materials reach levels of similar TON after 2 h of reaction. Additionally, the advantage of using carbonized materials in comparison to resins is clear both for resorcinol and tannin-based materials.

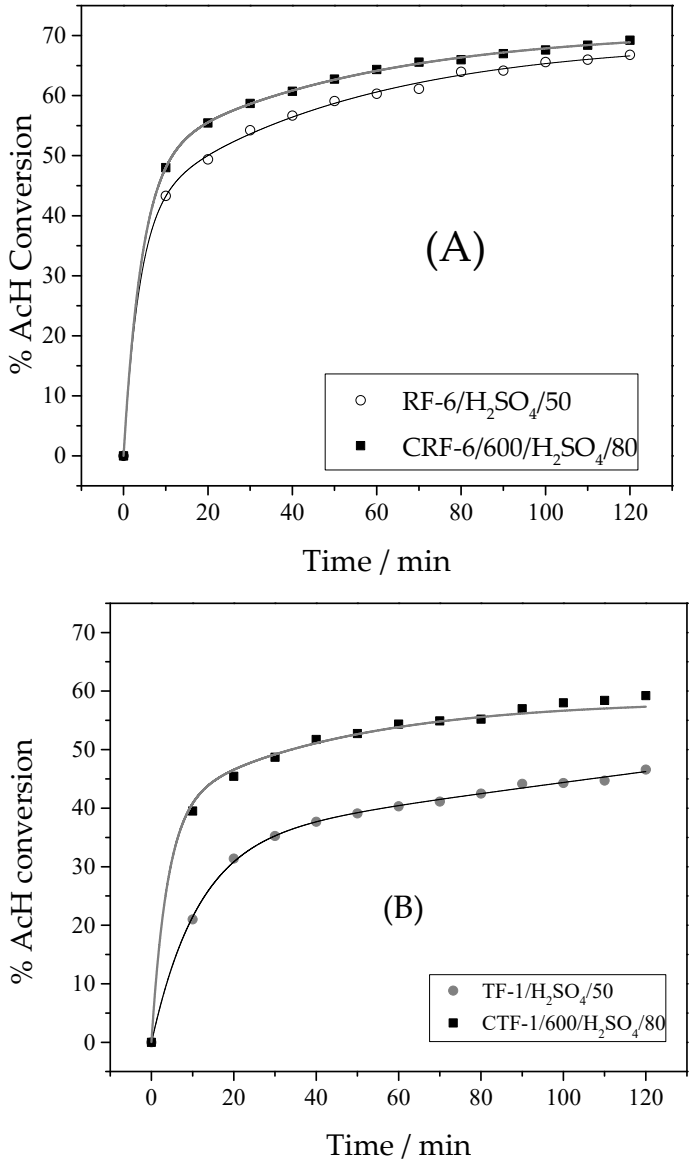

Figure 9. Acetic acid conversion curve as a function of time using resorcinol-based resin and carbon (**A**) and tannin-based resin and carbon (**B**) nanoparticles as acid catalysts. Reaction is Ficher esterification of acetic acid with methanol at 80 °C, using 0.1% *w*/*v* of catalyst.

The conversions achieved in the esterification reaction, in the presence of the different synthesized catalysts, as well as two commercial catalysts (Nafion 117 and Amberlite IR-120,

whose sulfonic group content is 0.9 mmol/g and 4.6 mmol/g, respectively) after two hours of reaction, are shown in Figure 11.

It can be seen that the conversions reached when commercial catalysts are used are lower than those reached with sulfonated nanoparticles. Accordingly, they reach the conversion plateau later, suggesting less access to the sulfonic acid sites. It should be remembered that both commercial materials are porous solids, while the catalysts synthesized here are nanoparticulated. It is likely that reactants show faster mass transport in the solution to the particles than through the porous carbon structure. On the other hand, highly porous sulfonated carbon materials can be used as catalysts of Fischer esterification and triglycerides transesterification [47]. However, the mass transport could be slow inside the porous structure compared to the transport in the nanoparticle dispersion (which can also be increased by fast stirring). Moreover, the dispersed nanoparticles can be used as photothermal catalysts, while the opaque bulk porous carbon materials cannot. These characteristics show great potential in their use as heterogeneous catalysts in Fischer esterification reactions, replacing commercial catalysts currently on the market. It is noteworthy that sulfonated polymers (especially Nafion®) are significantly more expensive and of much lower eco-sustainability than the sulfonated nanoparticles produced here (especially those made with renewable tannin).

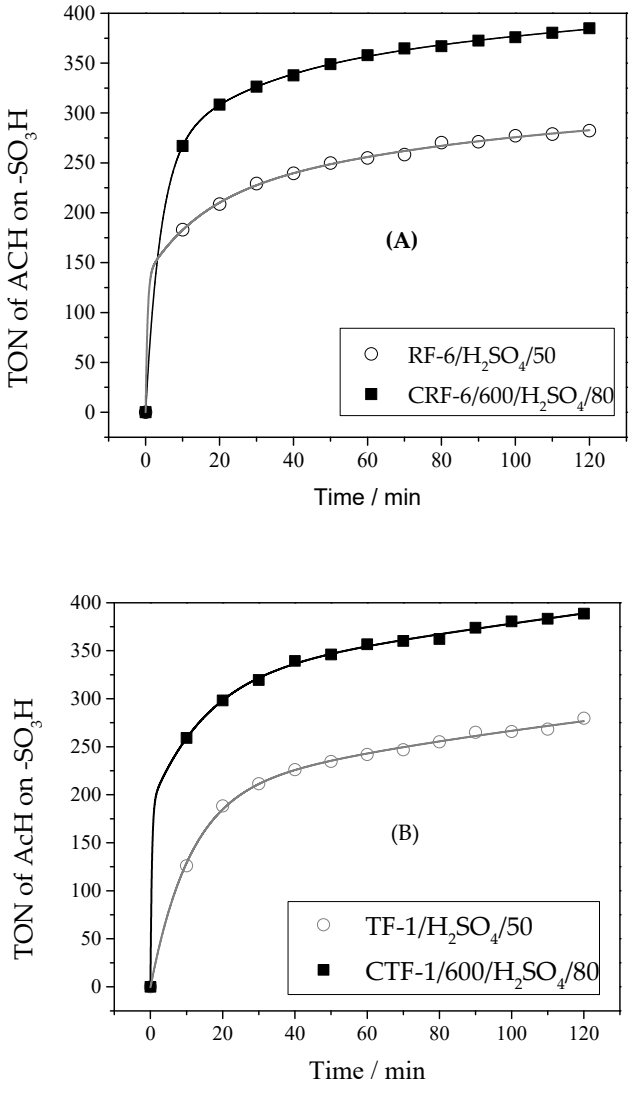

Figure 10. TON as a function of time for the esterification of acetic acid with methanol at 80 °C, 0.1% *w*/*v* of catalyst: (**A**) RF-6/H_2SO_4/50 and CRF-6/600/H_2SO_4/80, (**B**) TF-1/H_2SO_4/50 and CTF-1/600/H_2SO_4/80.

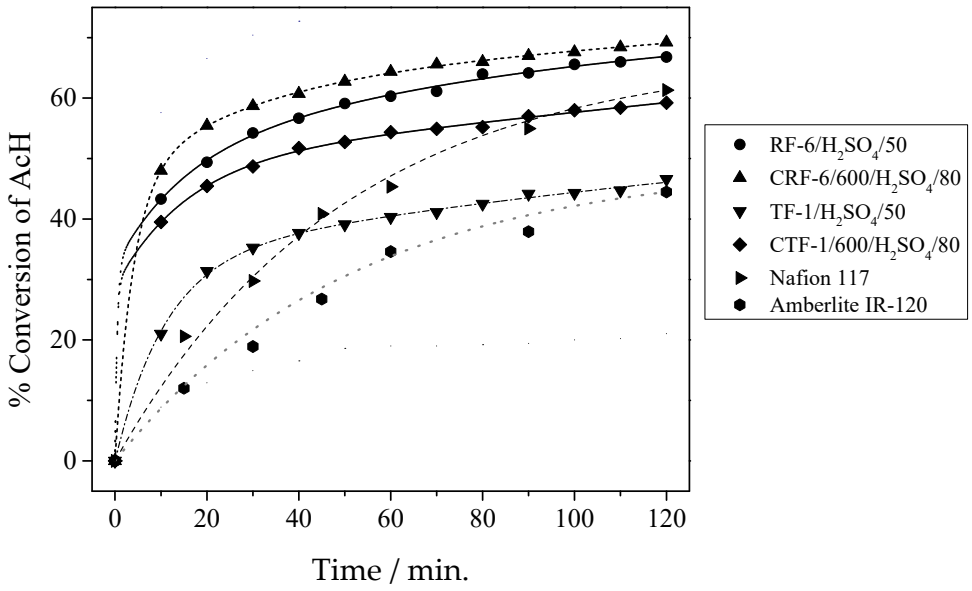

Figure 11. Acetic acid conversion curve as a function of time. Esterification of acetic acid with methanol at 80 °C, 0.1% w/v of solid catalysts: CRF-6/600, RF-6/H_2SO_4/50, CRF-6/600/H_2SO_4/80, TF-1/H_2SO^4/50, CTF-1/600/H_2SO_4/80 and Nafion 117 and Amberlite IR-120.

2.16. Photothermal Heating

Carbon nanoparticles should absorb strongly light across the UV–visible–NIR range. In Figure 12, the photothermal heating of carbon nanoparticle dispersion is shown. It can be seen that temperature increases upon irradiation. However, the local temperature at the catalyst surface should be higher, since the temperature of the whole dispersion is measured, and heat is transferred to the solution. Accordingly, it was observed that the photothermally induced temperature change is smaller when the particles are dispersed in water (Cv = 0.992 kcal kg^{-1} K^{-1}) than in methanol (Cv = 0.497 kcal kg^{-1} K^{-1}), suggesting that bulk temperature is measured, not those on the carbon surface.

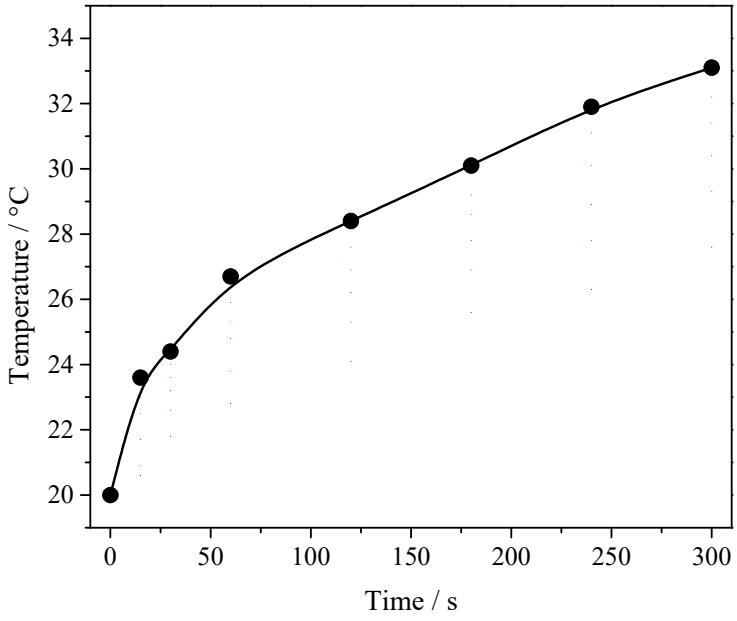

Figure 12. Dependence of temperature on irradiation time of CRF-6/600 nanoparticle dispersion in methanol. Irradiation was performed with a NIR (785 nm, 100 mW) laser.

3. Materials and Methods

3.1. Fabrication of Sulfonated Nanoparticles

3.1.1. Nanoparticle Synthesis

For the synthesis of polymer nanoparticles, two types of organic precursor systems were used: resorcinol (R) (Fluka) and formaldehyde (F) (Cicarelli, San Lorenzo, Argentina 37% *w*/*w*) to obtain RF resin nanoparticles and tannin (T) (Fabriquimica, CABA, Argentina) and formaldehyde to produce TF resin nanoparticles. In both systems, ammonium hydroxide (C) (Biopack, Santa Fe, Argentina, 25%) was used as a catalyst and the reaction medium consisted of a solution of distilled water (W) and ethanol, medicinal grade (EtOH) (Porta, Cordoba, Argentina, 96% *v*/*v*). The EtOH/W volumetric ratio and the concentration of catalyst C were maintained constants at values equal to 0.393 and 0.0529 M, respectively. The mole ratio F:R was kept constant at a value of 2:1 for all the materials synthesized from the RF systems; the ratio mass of tannin to the volume of formaldehyde (T:F), on the other hand, was kept at 0.475 g/mL. Once these synthesis conditions were set, only the mass ratio R:C or T:C was varied, depending on the precursor system. The resin nanoparticles obtained from resorcinol/formaldehyde were called RF-x and TF-x those obtained from tannin/formaldehyde, where x is the ratio in mass of precursor to catalyst (R:C or T:C, as appropriate).

For each of these syntheses, the reaction mixture was placed in a hermetic glass container, which was magnetically stirred for 24 h at 30 °C. Then, it was heated at 100 °C for 24 h in an autoclave, without stirring. The polymeric nanoparticles obtained were separated from the reaction medium by centrifugation and successive washings with distilled water and dried in an oven for 48 h at 100 °C.

Different samples of phenol (P)-formaldehyde (F) nanoparticles were synthesized by means of the Stöber method [37], The reaction conditions were as follows: molar ratio F:Ph (2:1), EtOH/W (water) volumetric ratio of 0.3725 and a concentration of catalyst C (NH_4OH) of 0.0529 M. The phenols (Ph) used are resorcinol (R) and Tannin (T Maintaining those parameters constant the mass ratio Ph:C was varied. Therefore, the resin nanoparticles were called RF-x, and the corresponding carbon nanoparticles were called CRF-x/Tp, where x is the P:C ratio, and Tp is the pyrolysis temperature. The mass ratio of tannin to volume of formaldehyde (T:F) was kept at 0.475 g/mL, and the resin nanoparticles obtained from tannin/formaldehyde and the corresponding carbon were called TF-x and CTF-x/Tp, respectively, where x is the ratio of mass of precursor T to the volume of the catalyst (ammonium hydroxide) (Table 12). In all cases, the temperature of synthesis was 30 °C.

Table 12. Synthetic conditions of the CRF-x/Tp and CTF-x/Tp materials.

Material	W (mL)	EtOH (mL)	C * (mL)	Ph (R or T) (g)	F (mL)	Ph:C
CRF-6/600	20.4	7.6	0.1	0.15	0.21	6
CRF-6/900	20.4	7.6	0.1	0.15	0.21	6
CRF-4/600	20.4	7.6	0.1	0.1	0.14	4
CRF-4/900	20.4	7.6	0.1	0.1	0.14	4
CRF-2/600	20.4	7.6	0.1	0.05	0.07	2
CRF-2/900	20.4	7.6	0.1	0.05	0.07	2
CTF-6/600	20.4	7.6	0.1	0.6	1.68	6
CTF-6/900	20.4	7.6	0.1	0.6	1.68	6
CTF-1.5/600	20.4	7.6	0.1	0.15	0.84	1.5
CTF-1.5/900	20.4	7.6	0.1	0.15	0.84	1.5
CTF-1/600	20.4	7.6	0.1	0.1	0.21	1
CTF-1/900	20.4	7.6	0.1	0.1	0.21	1

* Catalyst (ammonium hydroxide).

3.1.2. Carbonization of Resin Nanoparticles

The precursors obtained by the Stöber synthesis were subjected to pyrolysis to produce carbon nanospheres. Two carbonization cycles were used, in order to analyze the influence of parameters on the nanoparticle properties. The main carbonization cycle carried out in

an argon atmosphere consisted of two stages of heating alternated with two isothermal periods: heating at a rate of 1 °C/min up to 350 °C, isothermal period of 2 h at 350 °C, heating at a rate of 1 °C/min up to 600 °C, isothermal period of 4 h at 600 ° and finally cooling to room temperature. They were named CRF-x/600 and CTF-x/600 at carbon nanoparticles derived from RF-x and TF-x resins, respectively, resulting from this pyrolysis cycle. The heating rate was higher than the rate used for macroscopic resins, since the small size of the nanoparticles makes it easier for the gases produced during pyrolysis to escape.

3.1.3. Sulfonation of Resin and Carbon Nanoparticles

This functionalization method consists of direct exposure of the material to functionalize to concentrated sulfuric acid, with heating [25]. Electrophilic aromatic substitution of SO_3 (in equilibrium with sulfuric acid) on the aromatic rings of graphite domains, allows attachment of $–SO_3H$ groups, likely to the graphene borders and defects. The reaction was carried out both for the nanoparticles of resins synthesized by the Stöber method and for the carbons derived from the pyrolysis of the same, of both precursor systems (RF and TF). In the case of the resins, the aromatic rings bear groups (e.g., –OR) which activate the ring for electrophilic aromatic substitution. Moreover, the concentrated acid could hydrolyze the ether linkages in the crosslinked resins, degrading the material. Therefore, milder reaction conditions are used. A total of 2 g of sample was dispersed with ultrasound in 100 mL of concentrated H_2SO_4. Then, the solution was heated for only 15 min at 50 °C for resin NPs. On the other hand, the carbon NPs were allowed to react for 60 min at 80 °C. After the reaction time, the liquid was poured onto 100 g of ice to dilute the acid and cool to room temperature. Subsequently, the sulfonated particles were separated by centrifugation and dried in an oven at 100 °C for 48 h. Resin and carbon obtained were named RF-x/H_2SO_4/50 and CRF-x/Tp/H_2SO_4/80, respectively, in the case of the resorcinol-formaldehyde systems, and TF-x /H_2SO_4/50 and CTF-x/Tp/H_2SO_4/80 for the tannin-formaldehyde systems, where Tp is the pyrolysis temperature. Other sulfonation procedures were tested, such using fuming (30%) sulfuric acid or reacting with the diazonium salt of sulfanilic acid. No improvement in the sulfonation degree or catalytic activity was observed.

3.2. Characterization

3.2.1. Dynamic Light Scattering of Resin Nanoparticles

The resin particles were dispersed, at a very low concentration, in absolute ethanol (Biopack, 99.5%). The dynamic light scattering measurements were carried out using Malvern 4700 equipment with detection at 90° from the excitation, at a temperature of 22 °C, using the 488 nm spectral line of an argon ion laser. The results of dynamic light scattering were analyzed with the CONTIN software (supplied by the manufacturer) in order to obtain the distribution of hydrodynamic radii and the indices of polydispersity of the samples analyzed.

3.2.2. FE-SEM of Nanoparticles

The study of the morphology of the carbon nanoparticles samples was carried out using the FE-SEM method (field emission scanning electron microscopy) and a double-beam microscope (FEI Strata DB 235).

3.2.3. TEM of Nanoparticles

Transmission electron microscopy was used to determine morphology and size of the carbon particles obtained by the Stöber method. The study of morphology of the carbon samples was carried out using FEI TECNAI F20 equipment. This microscope has a field emission gun, which generates a beam of electrons of 200 keV with a high degree of coherence and allows imaging of up to 0.12 nm. This microscope also presents the possibility of obtaining a small and bright beam to capture images in scanning mode by means of a high angle ring detector. It allows us to distinguish the location of atoms of different weights and is called the contrast of atomic numbers. For the characterization in the transmission

electron microscope, the samples were prepared in four different ways: (1) Dispersion of 10 mg of CRF-x/600 in 1.5 mL of water. (2) Dispersion of 10 mg of CRF-x/600 in a barium chloride solution ($BaCl_2$) 0.1 M for 30 min, assisted by ultrasound. The samples were then centrifuged and washed and redispersed in 1.5 mL of water. (3) Dispersion of 10 mg of CRF-x/600/H_2SO_4/80 in 1.5 mL of water. (4) Dispersion of 10 mg of CRF-x/600/H_2SO_4/80 in a barium chloride solution ($BaCl_2$) 0.1 M for 30 min, assisted by ultrasound. The samples were then centrifuged and redispersed in 1.5 mL of water. The objective of treatment with barium chloride was to be able to map the sulphonic groups anchored to the surface of the particles, since they are detected more efficiently by EDX high atomic number atoms. Barium combines with sulfur to form sulphonates of barium, making it easier to determine the presence of these groups on the carbon surface [48]. The particles were dispersed on a copper grid for analysis.

3.2.4. Fourier-Transform IR (FTIR) Spectroscopy

FTIR spectra were taken using Nicolet Impact 400 equipment, with a resolution of 4 cm^{-1}. The materials were dispersed in dry KBr, and a pellet was produced applying a 10 Kg/cm^2 pressure.

3.2.5. Elemental Composition by EDX

The carbon samples were also characterized under a Scanning el3ectron Microscope (Carl Zeiss, Jena, FRG) equipped with a backscattered electron detector (BSE) and coupled to an EDX (energy-dispersive X-ray spectroscopy) system to identify the elemental composition of materials and the elemental mapping of the sample. The scanning electron microscope used is a Hitachi model S3000N (Osaka, Japan). This microscope has a Bruker (Dresden, FRG) model XFlash 3001 X-ray detector for microanalysis (EDX) and mapping.

3.2.6. Thermogravimetry (TGA)

The TGA measurements were carried out using TG 209 F1 Libra equipment, which has a resolution of 0.1 µg and can work in a range of heating and cooling rates between 0.001 K/min and 200 K/min. The initial temperature was 25 °C and rose at a rate of 10 °C/min, until reaching 500 °C, a temperature at which it was maintained for 15 min. Figure S2 (Supplementary Materials) shows two pyrolysis cycles used to carry out this analysis. The mass of sulfonic groups was obtained from the graph, taking into account that first the material experiences a loss of mass due to the water content and then due to the sulphonic groups.

3.2.7. Nitrogen Adsorption–Desorption Isotherms

The textural properties of the carbon catalysts synthesized by the Stöber method were evaluated by nitrogen adsorption-desorption measurements at −196 °C using automatic manometric equipment (N2Gsorb-G, Gas to Materials Technologies). The samples were previously dried and degassed for 8 h at 100 °C under dynamic vacuum. The S_{BET} of carbon samples obtained from RF resins was analyzed. The micropore size distribution was calculated by means of the density functional theory (DFT) considering pores slit-shaped [49].

3.2.8. Titrations

The content of sulfonic (-SO_3H) and other acidic groups (-OH, -COOH, lactonic) was determined by titration. The error of volumetric titration is 0.1 mL, which translates into a relative error of 2–5% in the determined content.

Determination of Sulfonic Groups

The content of sulfonic groups of the catalyst was determined by titration acid-base potentiometric. An aqueous solution of Na_2SO_4 (0.1 M, 20 mL) was added to 0.1 g of the synthesized catalyst, and the mixture was sonicated for 60 min at room temperature.

The objective of this process was to produce a reaction between the salt and sulphonic groups present in the solid catalyst, forming bisulphate. Other acid groups (carboxylic, phenolic, lactonic), present on the catalyst surface, are less acidic than sulfate and do not give bisulfate on exposure to the sulfate ions of the salt used. Once this operation was carried out, the suspension was centrifuged, and the supernatant solution was titrated with NaOH (0.2 M) using a glass electrode to measure the pH and stirring continuously during the titration. Bisulfate groups in solution react with the NaOH giving the total number of sulfonic acid groups. The standardization of the solution NaOH was performed using monoacid potassium phthalate as the primary standard. From the volume spent during the titration (V_{NaOH}), the number of sulfonic groups (nGS) is calculated.

Boehm Titration

The content of oxygenated (phenolic, lactonic and carboxylic acid groups) in the catalyst was determined by acid-base potentiometric titration using the standardized Boehm method [50,51]. The Boehm titration is based on the principle that the oxygenated groups present in the carbon surface have different acidity and can be neutralized by bases of different levels of alkalinity. The strongest base that is normally used to carry out this technique is sodium hydroxide (NaOH) since it is assumed to be capable of neutralizing all Brønsted acids (including sulphonic, phenolic, lactonic and carboxylic acid groups), while sodium carbonate (Na_2CO_3) neutralizes carboxylic, sulfonic and lactonic acid groups, and sodium bicarbonate ($NaHCO_3$) neutralizes carboxylic and sulfonic acids only. The difference between the affinity of the bases can be used to identify and quantify the types of oxygen surface groups present in a carbon sample [52]. Boehm's assessment must be standardized not only to maintain consistency between the results obtained but also to ensure that the methodology provides the most accurate results possible. A key point for this is to set a time and manner of the removal of carbon dioxide (CO_2) dissolved in the solutions to be titrated; another important matter is the way to determine the end point of the titration. The CO_2 dissolved in the solution has a significant effect on the number of functional groups determined by this method and therefore must be completely removed in order to ensure accuracy and precision. Since it is very complex to sufficiently remove CO_2 from the solutions used in a direct titration, it is convenient to carry out back titrations for each of the reaction bases; it is also beneficial to bubble the acidified solutions with an inert gas to remove CO_2. Based on this, the Boehm titration was standardized as follows: an amount of 1.5 g of catalyst sample was added to 50 mL of each of the three reaction bases with a concentration of 0.05 M: $NaHCO_3$, Na_2CO_3 and NaOH (Cicarelli). The samples were shaken on a magnetic stage for 24 h. Aliquots of 10 mL were taken of each one, which were subsequently acidified. The aliquots of the $NaHCO_3$ and NaOH reaction bases were made acidic by adding 20 mL of hydrochloric acid (HCl, Biopack, 37%) 0.05 M, while the aliquots of the Na_2CO_3 reaction base were acidified by adding 30 mL of 0.05 M HCl to ensure complete neutralization of the remaining base, which requires two protons per molecule, in front of the requirement of a proton by the other two bases used.

3.2.9. Catalysis of Fischer Esterification

The catalytic effect of sulfonated nanoparticles on Fischer esterification was determined by carrying out the esterification in the presence of the catalyst and measuring the conversion as a function of time. To achieve that, the amount of acetic acid remaining in the reaction media was determined by acid-base titration. Methanol in the amount of 50 mL (Cicarelli, p.a.) and glacial acetic acid (Fluka, p.a.) in the amount of 20 mL were placed in a 100 mL two-necked flask, with 0.07 g of catalyst (0.1% w/v). This mixture was sonicated for 15 min so that the catalyst was well dispersed in the liquid and then heated to reflux, maintaining the temperature constant at 80 °C and taking samples at regular periods of time. Immediately after taking the samples, 15 mL of distilled water was added to each sample to stop the reaction. Then, the samples were titrated to determine the degree of conversion of the reaction. The reaction kinetics was followed for a period of two hours,

taking 2 mL samples every 10 min. The remaining acetic acid content in the samples was determined by potentiometric acid-base titration with standardized KOH solutions using a glass electrode to measure the pH and stirring continuously during titration.

3.2.10. Thermogravimetric Analysis (TGA)

The thermogravimetric analysis was performed in a TGA (TG 209 F1 Libra, Netzch, Dresden, FRG) using aluminum crucibles.

3.2.11. Photothermal Heating

1 mL of carbon nanoparticle dispersion was placed inside an Eppendorf plastic tube. The dispersion was irradiated from the open top of the tube with a NIR laser (Ocean Optics, 785 nm, 100 mW) and the temperature measured at 90 °C with a handheld infrared thermometer. The temperature was also measured with a thermistor at the beginning and end of the experiment. Both measurements agree within an average of 2 °C).

4. Conclusions

It was demonstrated that the synthesis of polymeric resin nanoparticles is possible by the extension of the Stöber method, already tested with resorcinol-formaldehyde, to a sustainable phenolic precursor: tannin. The DLS measurements show the formation of resin nanoparticles (d < 600 nm) with low polydispersity. The resin nanoparticles can be carbonized by pyrolysis in an inert atmosphere (600 and 900 °C). The SEM and TEM micrographs show nanoparticles of spherical morphology, with sizes similar to those measured by DLS. The nitrogen adsorption-desorption isotherms confirmed that the synthesized materials do not present mesoporosity, and that the surface area, calculated by the BET theory, is basically given by the exposed area, that is, determined by the size of the nanoparticle. Through isotherms and TEM analysis, it can be stated that the pyrolysis cycle does not cause changes in the porosity and morphology of the material.

The nanoparticles can be functionalized by electrophilic aromatic sulfonation using concentrated sulfuric acid. The anchoring of sulfonic groups is ascertained by FTIR and EDX. The content of sulfonic groups was determined by acid-base potentiometric titration and the content of other acidic functional groups by Boehm titration. Resin nanoparticles show a higher content of sulfonic groups, compared to carbon nanoparticles. Materials synthesized from resorcinol-formaldehyde exhibit a higher level of sulfonation than those synthesized from tannin-formaldehyde. The degree of sulfonation is higher for carbons produced at lower pyrolysis temperature (600 °C). Complementary studies by SEM-EDX revealed that sulfonation occurs uniformly on the surface of the studied materials. A comparison of the nitrogen adsorption-desorption isotherms, show little changes due to sulfonation. The sulfonated nanoparticles are efficient as catalysts for Fischer esterification with performances that exceed commercial catalysts. The effectiveness of the sulfonic groups in the different materials was evaluated for an esterification reaction (acetic acid with ethanol). The catalytic activity is compared to those exhibited by nonfunctionalized carbons, whose active sites are mainly constituted by carboxylic acids. The results obtained indicate that the conversion achieved by these materials is much lower than that available with sulfonated materials, indicating that sulfonate groups are effective in catalyzing this type of reaction, allowing conversions close to 70% to be achieved in a period of 2 h. This kinetic study (% conversion vs. time) shows that the resorcinol-based resin materials are more active than those based on tannin. However, the evolution of turnover numbers (moles of acetic acid converted per moles of sulfonic groups) show that both materials are quite similar, suggesting that the number of sulfonic groups explain the differences observed in the kinetic experience. A comparison of sulfonated resin and carbon nanoparticles shows that most materials are better acidic catalysts than sulfonated polymers (Nafion® and Amberlite 150). On the other hand, the sulfonated carbon made by pyrolysis of RF resin nanoparticles show a lower activity. In Part II of this publication, the study of catalytic effect is extended to the synthesis of biodiesel by transesterification

of sunflower oil with methanol and ethanol. Different parameters of the reaction, such as the effect of catalyst amount, reaction temperature, reaction time and oil/alcohol ratio are measured. Then, the activation energy of the Fischer esterification and transesterification is measured. The photothermal heating of the sulfonated carbon nanoparticles is also determined. Finally, the photothermal catalysis by sulfonated carbon nanoparticles of the esterification of acetic acid with methanol and the transesterification of sunflower oil with ethanol is demonstrated.

Supplementary Materials: The following supporting information can be downloaded at https://www.mdpi.com/article/10.3390/catal13101341/s1. Figure S1: Potentiometric titration curves; Figure S2: Heating ramps; Figure S3: Heating ramp for TGA; Figure S4 Potentiometric titration curves; Figure S5: EDX spectrum; Figure S6: SEM micrograph of CRF-6/600; Figure S7: SEM micrograph of CRF-6/600/H_2SO_4/80; Figure S8: SEM micrograph of CTF-1/600; Figure S9: SEM micrograph of CTF-1/600/H_2SO_4/80; Figure S10: Potentiometric back titration curves of materials treated with treated with 0.05 NaOH M and 0.05 M HCl; Figure S11: Potentiometric back titration curves of materials treated with Na_2CO_3 0.05 M and 0.05 M HCl; Figure S12: Potentiometric back titration curves of materials, treated with 0.05 $NaHCO_3$ M and 0.05 M HCl

Author Contributions: Conceptualization, C.A.B. and D.F.A.; methodology, M.P.M. and L.T.; formal analysis, M.P.M., M.V.M., C.A.B. and D.F.A.; investigation, M.P.M. and C.A.B.; resources, C.A.B.; data curation, C.A.B.; writing—original draft preparation, M.P.M. and C.A.B., writing—review and editing, C.A.B.; supervision, D.F.A. and C.A.B., project administration, C.A.B.; funding acquisition, C.A.B. All authors have read and agreed to the published version of the manuscript.

Funding: This research was funded by FONCYT (PICT 2450/2019 and PICT II Salto Institucional 6/2021), CONICET (PUE of IITEMA) and SECYT-UNRC (PICT SSPR).

Acknowledgments: C.A.B., D.F.A., M.V.M. and M.P.M. are permanent researchers of CONICET. Technical support from the Advanced Materials Laboratory (LMA) of the University of Alicante (Alicante, Spain) (FE-SEM and N_2 adsorption-desorption isotherms measurements) and the Nanoscience and Nanotechnology Institute (Node Bariloche, Argentina) (FE-SEM-EDX and TEM measurements) is gratefully acknowledged.

Conflicts of Interest: The authors declare no conflict of interest. The funders had no role in the design of this study; in the collection, analyses or interpretation of data; in the writing of the manuscript; or in the decision to publish the results.

References

1. Leung, D.Y.; Wu, X.; Leung, M.K.H. A review on biodiesel production using catalyzed transesterification. *Appl. Energy* **2010**, *87*, 1083. [CrossRef]
2. Avhad, M.; Marchetti, J. Innovation in solid heterogeneous catalysis for the generation of economically viable and ecofriendly biodiesel: A review. *Catal. Rev. Sci. Eng.* **2016**, *58*, 157. [CrossRef]
3. Wang, B.; Wang, B.; Shukla, S.K.; Wang, R. Enabling Catalysts for Biodiesel Production via Transesterification. *Catalysts* **2023**, *13*, 740. [CrossRef]
4. Chandra Kishore, S.; Perumal, S.; Atchudan, R.; Sundramoorthy, A.K.; Alagan, M.; Sangaraju, S.; Lee, Y.R. A Review of Biomass-Derived Heterogeneous Catalysts for Biodiesel Production. *Catalysts* **2022**, *12*, 1501. [CrossRef]
5. Nisar, S.; Hanif, M.A.; Rashid, U.; Hanif, A.; Akhtar, M.N.; Ngamcharussrivichai, C. Trends in Widely Used Catalysts for Fatty Acid Methyl Esters (FAME) Production: A Review. *Catalysts* **2021**, *11*, 1085. [CrossRef]
6. Chouhan, A.P.S.; Sarma, A.K. Modern heterogeneous catalysts for biodiesel production: A comprehensive review. *Renew. Sust. Energ. Rev.* **2011**, *15*, 4378. [CrossRef]
7. Alsultan, A.G.; Asikin-Mijan, N.; Ibrahim, Z.; Yunus, R.; Razali, S.Z.; Mansir, N.; Islam, A.; Seenivasagam, S.; Taufiq-Yap, Y.H. A Short Review on Catalyst, Feedstock, Modernised Process, Current State and Challenges on Biodiesel Production. *Catalysts* **2021**, *11*, 1261. [CrossRef]
8. Hájek, M.; Vávra, A.; de Paz Carmona, H.; Kocík, J. The Catalysed Transformation of Vegetable Oils or Animal Fats to Biofuels and Bio-Lubricants: A Review. *Catalysts* **2021**, *11*, 1118. [CrossRef]
9. Estevez, R.; Aguado-Deblas, L.; Bautista, F.M.; Luna, D.; Luna, C.; Calero, J.; Posadillo, A.; Romero, A.A. Biodiesel at the Crossroads: A Critical Review. *Catalysts* **2019**, *9*, 1033. [CrossRef]
10. Damera, T.; Pagadala, R.; Rana, S.; Jonnalagadda, S.B. A Concise Review of Multicomponent Reactions Using Novel Heterogeneous Catalysts under Microwave Irradiation. *Catalysts* **2023**, *13*, 1034. [CrossRef]

11. Kulkarni, M.G.; Gopinath, R.; Meher, L.C.; Dalai, A.K. Solid acid catalyzed biodiesel production by simultaneous esterification and transesterification. *Green Chem.* **2006**, *8*, 1056–1062. [CrossRef]
12. Zabeti, M.; Wan Daud, W.M.A.; Aroua, M.K. Activity of solid catalysts for biodiesel production: A review. *Fuel Process. Technol.* **2009**, *90*, 770. [CrossRef]
13. Van Gerpen, J. Biodiesel processing and production. *Fuel Process. Technol.* **2005**, *86*, 1097. [CrossRef]
14. Klepacova, K.; Mravec, D.; Bajus, M. Etherification of glycerol with tert-butyl alcohol catalysed by ion-exchange resins. *Chem. Pap.* **2006**, *60*, 224. [CrossRef]
15. Twaiq, F.A.; Mohamad, A.; Bhatia, S. Performance of composite catalysts in palm oil cracking for the production of liquid fuels and chemicals. *Fuel Process. Technol.* **2004**, *85*, 1283–1300. [CrossRef]
16. Lopez, D.E.; Goodwin, J.G.; Bruce, D.A. Transesterification of triacetin with methanol on Nafion_ acid resins. *J. Catal.* **2007**, *245*, 381. [CrossRef]
17. Twaiq, F.A.; Mohamed, A.R.; Bhatia, S. Liquid hydrocarbon fuels from palm oil by catalytic cracking over aluminosilicate mesoporous catalysts with various Si/Al ratios. *Microporous Mesoporous Mater.* **2003**, *64*, 95. [CrossRef]
18. Zuo, D.; Lane, J.; Culy, D.; Schultz, M.; Pullar, A.; Waxman, M. Sulfonic acid functionalized mesoporous SBA-15 catalysts for biodiesel production. *Appl. Catal. B Environ.* **2013**, *129*, 342. [CrossRef]
19. Konwar, L.J.; Mäki-Arvela, P.; Mikkola, J.-P. SO_3H-Containing Functional Carbon Materials: Synthesis, Structure, and Acid Catalysis. *Chem. Rev.* **2019**, *119*, 11576. [CrossRef]
20. Vakros, J. Biochars and Their Use as Transesterification Catalysts for Biodiesel Production: A Short Review. *Catalysts* **2018**, *8*, 562. [CrossRef]
21. Fonseca, J.M.; Spessato, L.; Cazetta, A.L.; da Silva, C.; Almeida, V.D.C. Sulfonated carbon: Synthesis, properties and production of biodiesel. *Chem. Eng. Process.* **2022**, *170*, 108668. [CrossRef]
22. Lowe, B.; Gardy, J.; Hassanpour, A. The Role of Sulfated Materials for Biodiesel Production from Cheap Raw Materials. *Catalysts* **2022**, *12*, 223. [CrossRef]
23. Deris, N.H.; Rashid, U.; Soltani, S.; Choong, T.S.Y.; Nehdi, I.A. Study the Effect of Various Sulfonation Methods on Catalytic Activity of Carbohydrate-Derived Catalysts for Ester Production. *Catalysts* **2020**, *10*, 638. [CrossRef]
24. Qi, K.; Sun, B.; Liu, S.-Y.; Zhang, M. Research progress on carbon materials in tumor photothermal therapy. *Biomed. Pharmacother.* **2023**, *165*, 115070. [CrossRef] [PubMed]
25. Wei, C.; Jin, X.; Wu, C.; Brozovic, A.; Zhang, W. Carbon spheres with high photothermal conversion efficiency for photothermal therapy of tumor). *Diam. Relat. Mater.* **2022**, *126*, 109048. [CrossRef]
26. Tamborini, L.; Militello, P.; Barbero, C.; Acevedo, D. Production of porous carbons from resorcinol-formaldehyde gels: Applications. In *Handbook of Composites from Renewable Materials*; John Wiley & Sons: Hoboken, NJ, USA, 2017; pp. 175–196. [CrossRef]
27. Nguyen, H.C.; Nguyen, M.-L.; Su, C.-H.; Ong, H.C.; Juan, H.-Y.; Wu, S.-J. Bio-Derived Catalysts: A Current Trend of Catalysts Used in Biodiesel Production. *Catalysts* **2021**, *11*, 812. [CrossRef]
28. Bucciol, F.; Colia, M.; Calcio Gaudino, E.; Cravotto, G. Enabling Technologies and Sustainable Catalysis in Biodiesel Preparation. *Catalysts* **2020**, *10*, 988. [CrossRef]
29. China, C.R.; Hilonga, A.; Nyandoro, S.S.; Schroepfer, M.; Kanth, S.V.; Meyer, M.; Njau, K.N. Suitability of selected vegetable tannins traditionally used in leather making in Tanzania. *J. Clean. Prod.* **2020**, *251*, 119687. [CrossRef]
30. Tondi, G.; Fierro, V.; Pizzi, A.; Celzard, A. Tannin-based carbon foams. *Carbon* **2009**, *47*, 1480. [CrossRef]
31. Romero-Dondiz, E.M.; Almazán, J.E.; Rajal, V.B.; Castro-Vidaurre, E.F. Removal of vegetable tannins to recover water in the leather industry by ultrafiltration polymeric membranes. *Chem. Eng. Res. Des.* **2015**, *93*, 727. [CrossRef]
32. Porter, L.J. Flavans and Proanthocyanidins. In *The Flavonoids*; Springer: Berlin/Heidelberg, Germany, 1988; pp. 21–62.
33. Pizzi, A.; Tondi, G.; Pasch, H.; Celzard, A. Matrix-assisted laser desorption/ionization time-of-flight structure determination of complex thermoset networks: Polyflavonoid tannin-furanic rigid foams. *J. Appl. Polym. Sci.* **2008**, *110*, 1451. [CrossRef]
34. Szczurek, A.; de Yuso, A.M.; Fierro, V.; Pizzi, A.; Celzard, A. Tannin-based monoliths from emulsion-templating. *Mater. Des.* **2015**, *79*, 115. [CrossRef]
35. Kraiwattanawong, K.; Mukai, S.; Tamon, H.; Lothongkum, A. Preparation of carbon cryogels from wattle tannin and furfural. *Microporous Mesoporous Mater.* **2007**, *98*, 258. [CrossRef]
36. Ahmed, W.; Jeidi, H.; Djeridi, W.; Ben Mansour, N.; Llewellyn, P.L.; Dahman, H.; El Mir, L. Pyrolysis temperature effect on electrical properties and ethane storage capacity of bimodal porous synthetic carbon. *Ind. J. Phys.* **2023**, *97*, 1769. [CrossRef]
37. Stöber, W.; Fink, A.; Bohn, E. Controlled growth of monodisperse silica spheres in the micron size range. *J. Colloid Interface Sci.* **1968**, *26*, 62. [CrossRef]
38. Grün, M.; Lauer, I.; Unger, K.K. The synthesis of micrometer- and submicrometer-size spheres of ordered mesoporous oxide MCM-41. *Adv. Mater.* **1997**, *9*, 254. [CrossRef]
39. Green, D.L.; Lin, J.S.; Lam, Y.-F.; Hu, M.Z.-C.; Schaefer, D.W.; Harris, M.T. Size, volume fraction, and nucleation of Stober silica nanoparticles. *J. Colloid. Interface Sci.* **2003**, *266*, 346. [CrossRef]
40. Liu, J.; Qiao, S.Z.; Liu, H.; Chen, J.; Orpe, A.; Zhao, D.; Lu, G.Q. Extension of the Stöber method to the preparation of monodisperse resorcinol-formaldehyde resin polymer and carbon spheres. *Angew. Chem.* **2011**, *50*, 5947–5951. [CrossRef]

41. Lu, A.H.; Hao, G.P.; Sun, Q. Can Carbon Spheres Be Created through the Stöber Method? *Angew. Chem. Int. Ed.* **2011**, *50*, 9023. [CrossRef]
42. Bruno, M.M.; Cotella, N.G.; Miras, M.C.; Koch, T.; Seidler, S.; Barbero, C. Characterization of monolithic porous carbon prepared from resorcinol/formaldehyde gels with cationic surfactant. *Colloids Surf. A Physicochem. Eng. Asp.* **2010**, *358*, 13. [CrossRef]
43. Socrates, G. *Infrared and Raman Characteristic Group Frequencies: Tables and Charts*; John Wiley & Sons: Hoboken, NJ, USA, 2004.
44. Aldana-Pérez, A.; Lartundo-Rojas, L.; Gómez, R.; Niño-Gómez, M. Sulfonic groups anchored on mesoporous carbon Starbons-300 and its use for the esterification of oleic acid. *Fuel* **2012**, *100*, 128–138. [CrossRef]
45. Nakajima, K.; Okamura, M.; Kondo, J.N.; Domen, K.; Tatsumi, T.; Hayashi, S.; Hara, M. Amorphous carbon bearing sulfonic acid groups in mesoporous silica as a selective catalyst. *Chem. Mater.* **2008**, *21*, 186–193. [CrossRef]
46. Margolese, D.; Melero, J.; Christiansen, S.; Chmelka, B.; Stucky, G. Direct syntheses of ordered SBA-15 mesoporous silica containing sulfonic acid groups. *Chem. Mater.* **2000**, *12*, 2448. [CrossRef]
47. Björk, E.M.; Militello, M.P.; Tamborini, L.H.; Coneo Rodriguez, R.; Planes, G.A.; Acevedo, D.F.; Moreno, M.S.; Odén, M.; Barbero, C.A. Mesoporous silica and carbon based catalysts for esterification and biodiesel fabrication—The effect of matrix surface composition and porosity. *Appl Catal A-Gen.* **2017**, *533*, 49–58. [CrossRef]
48. Boothroyd, C.B.; Moreno, M.S.; Duchamp, M.; Kovács, A.; Monge, N.; Morales, G.M.; Barbero, C.A.; Dunin-Borkowski, R.E. Atomic resolution imaging and spectroscopy of barium atoms and functional groups on graphene oxide. *Ultramicroscopy* **2014**, *145*, 66–73. [CrossRef]
49. Barrett, E.P.; Joyner, L.G.; Halenda, P.P. The determination of pore volume and area distributions in porous substances. I. Computations from nitrogen isotherms. *J. Amer. Chem. Soc.* **1951**, *73*, 373–380. [CrossRef]
50. Bottani, E.J.; Tascón, J.M. *Adsorption by Carbons: Novel Carbon Adsorbents*; Elsevier: Amsterdam, The Netherlands, 2011.
51. Hao, H.; Shen, F.; Yang, J.; Qiu, M.; Guo, H.; Qi, X. Synthesis of Sulfonated Carbon from Discarded Masks for Effective Production of 5-Hydroxymethylfurfural. *Catalysts* **2022**, *12*, 1567. [CrossRef]
52. Delhaes, P. *Graphite and Precursors*; CRC Press: Boca Raton, FL, USA, 2000.